

Article

Poisoning Effect of SO₂ on Honeycomb Cordierite-Based Mn–Ce/Al₂O₃ Catalysts for NO Reduction with NH₃ at Low Temperature

Chengzhi Wang ¹ , Cheng Zhang ¹, Yonggang Zhao ¹, Xin Yan ² and Peng Cao ^{1,*}

¹ Key Laboratory for Green Processing of Chemical Engineering of Xinjiang Bingtuan, School of Chemistry and Chemical Engineering, Shihezi University, Shihezi 832003, China; wangchengzhihh@163.com (C.W.); zhangcheng137931@163.com (C.Z.); zhaoyonggang0106@163.com (Y.Z.)

² Tianfu South Thermoelectric Co., Ltd., Shihezi 832000, China; tfyx@163.com

* Correspondence: caop@shzu.edu.cn

Received: 30 November 2017; Accepted: 8 January 2018; Published: 11 January 2018

Abstract: Honeycomb cordierite-based Mn–Ce/Al₂O₃ catalysts were prepared by the impregnation method and used for low-temperature selective catalytic reduction (SCR) of NO_x with NH₃, with and without SO₂ and/or H₂O in a homemade fixed-bed tubular reactor. The catalyst reached nearly 80% NO_x conversion at 100 °C in the absence of SO₂. However, SO₂ reduces the catalytic activity (80% to 72%) of the honeycomb cordierite-based Mn–Ce/Al₂O₃ catalysts under identical conditions. This finding demonstrated that the catalyst exhibited high activity at low temperature and excellent SO₂ resistance in the presence of 50 ppm SO₂. The fresh and sulfated honeycomb cordierite-based Mn–Ce/Al₂O₃ catalysts were characterized by scanning electron microscopy (SEM), energy dispersive spectroscopy (EDS), N₂ adsorption–desorption, X-ray diffraction (XRD), X-ray photoelectron spectroscopy (XPS), thermogravimetry and differential thermal analysis (TG-DTA), and Fourier transform infrared (FT-IR) spectroscopy. Characterization results indicated that the deactivation by SO₂ was primarily the result of the deposition of ammonium hydrogen sulfate and sulfated CeO₂ on the catalyst surface during the SCR process. The formed sulfates depressed the catalytic activity via the blocking of pores and the occupation of active sites. Additionally, the competitive adsorption between SO₂ and NH₃ always decreased the catalytic activity.

Keywords: Mn–Ce/Al₂O₃ catalyst; low temperature selective catalytic reduction; honeycomb cordierite; SO₂ resistance

1. Introduction

Nitrogen oxides (NO_x) are global air pollutants, resulting from high-temperature combustion processes and adverse poisons in the atmosphere [1–3], including nitrogen monoxide (NO), nitrogen dioxide (NO₂), nitrous oxide (N₂O), and their derivatives, which have a wide range of health and environmental impacts. Selective catalytic reduction (SCR) of NO_x with NH₃ is an advanced, economic, and fuel-efficient technology that allows the removal of NO_x from stationary sources [4]. SCR can not only alleviate NO_x emissions by more than 90%, but can also concurrently reduce carbon monoxide emissions by 50–90%, and particulate matter emissions by 30–50%. V₂O₅–WO₃/TiO₂ and V₂O₅–MoO₃/TiO₂ have been widely used as commercial SCR catalysts [5,6]. However, their operating temperature (300–400 °C) limits the location of the SCR reactor to upstream from the electrostatic precipitator and desulfurizer [7,8]. This limitation causes some problems, such as the tendency to catalyze the rapid oxidation of SO₂ to SO₃, the corrosion of the downstream devices, and high concentrations of particulates and SO₂ in the flue gases, which shorten the life of the catalyst [9]. To avoid these adverse effects, it has been suggested that the SCR reactor could be located downstream

of the particle control and desulfurizer devices where the flue gas temperature is typically below 150 °C. In particular, after the wet desulfurization process, the flue gas will be cool, even below 100 °C [10,11]. A low-temperature SCR unit could be located downstream of the particulate control device and desulfurizer without heating, which results in low system energy consumption and ease of retrofitting into the boiler system; this would eliminate the need to reheat the stack gas, thus increasing the operational lifetime of the catalyst. Therefore, it is urgent to develop low-temperature SCR catalysts with high activity, high stability, a broad range of operating temperatures, and good SO₂ resistance.

Manganese oxides (MnO_x) have been extensively studied and proven to be highly active for low-temperature SCR of NO with NH₃ since they contain various types of labile oxygen species, which are essential for completing the catalytic cycle [12–16]. Researchers have also developed various Mn-based catalysts, such as MnO_x/Al₂O₃ [15], MnO_x/TiO₂ [16,17] and Mn–Ce–SnO₂ [18]. In addition, small concentrations of SO₂ remain in the flue gases after the desulfurizer, thus requiring consideration of the effect of SO₂ on activity. Many researchers [19–21] have shown that SO₂ has an apparent passivation effect on the catalytic activity of manganese oxide at low temperatures. Jin et al. [20,21] used the addition of CeO₂ to modified Mn/TiO₂ to significantly enhance the SO₂ poisoning resistance because CeO₂ can generate highly thermally stable Ce₂(SO₄)₃ and Ce(SO₄)₂, which prevent the formation of Mn(SO₄)_x and inhibit the deposition of NH₄HSO₄ and (NH₄)₂SO₃. However, the majority of catalysts for the preparation are in granular or powder form, which are unable to meet the needs of industrial applications due to the large bed pressure decrease and unequal surface distribution of the reactants in the catalyst. Limited research has focused on studying the mechanism of the effect, at pilot-scale, of a low concentration of SO₂ on honeycomb cordierite-based Mn–Ce/Al₂O₃ catalysts at 100 °C [3,7]. To realize the industrial application of an SCR unit located downstream of the particulate control device and desulfurizer without heating, it is advantageous to study the SO₂ resistance of the honeycomb catalyst at 100 °C. In addition, in order to be closer to the real conditions of industrial application, an industrial experiment platform device was built to test the effect of the honeycomb cordierite-based Mn–Ce/Al₂O₃ catalyst in Shihezi Tianfunan Thermoelectric Co., Ltd. (Xin Jiang, China). Before the industrial experiment platform test, the experiment was conducted in the laboratory according to the experimental conditions of the industrial experiment platform test. This experiment adopts an industrial-grade raw material preparation of the honeycomb cordierite-based Mn–Ce/Al₂O₃ catalyst in the lab as an enlargement of the pilot-scale experiment, for exploring the catalyst performance under the condition of simulating actual flue gas and the effects of SO₂ on SCR activities at low temperature. The physical and chemical properties were characterized in order to explore the reaction mechanism and provide theoretical support for the denitration catalyst at low temperatures in industrial applications.

2. Materials and Methods

2.1. Catalyst Preparation

The Mn–Ce/Al₂O₃ catalyst powder was prepared by the coprecipitation method (Mn/Ce/Al molar ratio of 2:3:1) using manganese nitrate, cerium nitrate, and aluminum nitrate as precursors. First, a fixed quantity of Al(NO₃)₃·9H₂O (Aladdin, Shanghai, China) was dissolved in distilled water with stirring. Then, prescribed amounts of Ce(NO₃)₃·6H₂O (Aladdin, Shanghai, China) and Mn(NO₃)₂·4H₂O (50%, Aladdin, Shanghai, China) were added to the above solution. The mixed solution was vigorously stirred for 2 h, and then slowly added into excess ammonia with stirring until the solution reached pH 10 and aged for 24 h, followed by washing until the pH remained stable. The sample was then dried at 110 °C for 12 h and calcined at 550 °C for 5 h. The catalyst was crushed and sieved to 150 mesh. Finally, impregnation was used to load the catalyst powder in the cordierite honeycomb carrier (Zhonghui Honeycomb Ceramics Ltd., Taicang, Jiangsu, China). Poly vinyl alcohol (GRACE, Tianjin, China), emulsifier (OP-10) (Aladdin, Shanghai, China), and sodium silicate (Aladdin, Shanghai, China) were dissolved in distilled water to form a solution and stirred for 1 h,

then slowly added into the catalyst powder with stirring for 0.5 h. Then, the support and mixed solutions were stirred for a further 10 min. After impregnation, the resulting material was dried at 110 °C for 6 h, followed by calcination at 500 °C for 3 h in air. The loading amount of Mn–Ce/Al₂O₃ was 15 wt %. For convenience, the honeycomb cordierite-based Mn–Ce/Al₂O₃ catalyst before the reaction was denoted F-Mn–Ce/Al₂O₃, while the catalyst after reaction without SO₂ and with SO₂ (50 ppm) for 24 h were denoted as R-Mn–Ce/Al₂O₃ and S-Mn–Ce/Al₂O₃, respectively.

2.2. Catalytic Activity Evaluation

The catalyst reaction was performed in a homemade fixed-bed tubular reactor (inner diameter 150 mm) at 100 °C containing 4 pieces of catalyst (catalyst specification: 100 mm (length) × 100 mm (width) × 150 mm (height), a honeycomb support with a channel density of 160 cells per square inch and a wall thickness of 0.5 mm). The premixed simulated gases (200 ppm NO, 200 ppm NH₃, 50 ppm SO₂ (when used) and 5 vol % H₂O (when used) with the balance air) were introduced into the reactor with a gas flow rate of 167 L/min, corresponding to a gas hour space velocity (GHSV) of 1667 h⁻¹. The concentration of NO was measured using a flue gas analyser (Testo 350, Lenzkirch, Germany).

2.3. Catalyst Characterization

Scanning electron microscopy (SEM) was used to observe the surface microstructure (XL-30ESEM, Phillips, Amsterdam, The Netherlands). Energy dispersive spectroscopy (EDS) was carried out on an X-MAXN 80TLE windowless EDS (Oxford Instruments, Oxford, UK) to get the dispersion of the metal on the catalyst surface by EDS elemental mapping. Specific surface areas, pore volume, and pore size distribution of the catalyst were measured by nitrogen adsorption at 77 K (Micrometrics ASAP-2020 Analyzer, Micro-meritics, Norcross, GA, USA) using the Brunauer–Emmet–Teller (BET) method. Before each adsorption measurement, approximately 0.3 g of the sample was degassed in N₂ at 300 °C for 4 h. X-ray powder diffraction (XRD) was performed to elucidate the crystal phase structure (Rigaku D/MAX RA) with Cu K_α radiation operated at 40 kV and 100 mA. The intensity data were collected in the range of 10–80°. Photoelectron spectroscopy (XPS) was used to analyse the surface atomic state of the catalyst with Al K_α X-rays (Thermo ESCALAB 250, Thermo Fisher Scientific, Waltham, MA, USA). The sample charging effects were compensated by calibrating all binding energies (BE) with the adventitious C1s line at 284.6 eV. The concentrations of Mn, Ce, O, and S on the catalyst surface were calculated from the peak intensity. Thermogravimetry differential thermal analysis (TG-DTA) of the samples was performed (NetzschThermoAnalyzer STA 449C, Netzsch, Waldkraiburg, Bavarian State, Germany) with a heating rate of 10 °C·min⁻¹ in flowing air. Fourier transform infrared (FT-IR) spectroscopy was performed using a Bruker Vector Fourier transform infrared spectrometer. The FT-IR spectra were recorded over the 800–4000 cm⁻¹ range to determine the sulfate and ammonium groups on the catalyst surface.

3. Results and Discussion

3.1. NH₃-SCR Activity Results

The effects of temperature on the SCR activities of the honeycomb cordierite-based Mn–Ce/Al₂O₃ catalyst are illustrated in Figure 1. The activities of the catalyst achieved more than 80% NO conversion at 100 °C, which is maintained at almost 100% over the entire 150–180 °C range. Furthermore, the catalyst exhibited excellent low-temperature NH₃-SCR activity which enlarged the active temperature window of the catalyst. Considering the energy consumption of flue gas reheating and catalyst efficiency in practical applications, the effects of SO₂ and H₂O were studied at 100 °C.

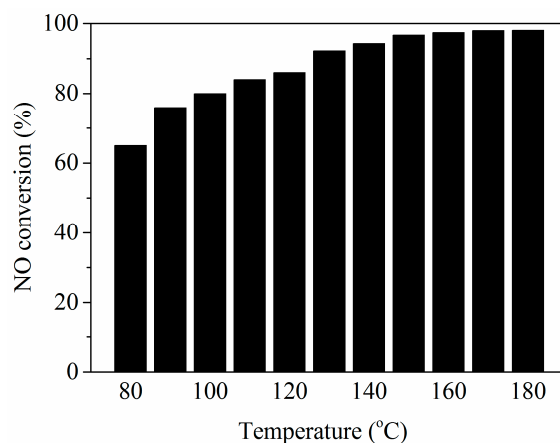


Figure 1. NO conversion by Mn–Ce/Al₂O₃ catalyst as a function of temperature. Reaction conditions: 200 ppm NO, 200 ppm NH₃, air balance, gas hour space velocity (GHSV) = 1667 h^{−1}.

3.2. Effects of SO₂ and H₂O on NO Removal Activity

In real applications in coal-fired power plants, small concentrations of H₂O and SO₂ still remain in the flue gas after the electrostatic precipitator and desulphurization devices. Therefore, the combined effect of SO₂ and H₂O should be considered for the SCR reaction. To explore the SO₂ and H₂O effects on the honeycomb cordierite-based Mn–Ce/Al₂O₃ catalyst in terms of NO removal efficiency, transient response experiments were performed at 100 °C. Figure 2a shows the results of the catalytic activity in the presence of SO₂ (50 ppm) over Mn–Ce/Al₂O₃. In the absence of SO₂, the steady-state NO conversion over the Mn–Ce/Al₂O₃ was approximately 80%, indicating that the catalyst has high activity at low temperature. After SO₂ (50 ppm) was introduced, NO conversion decreased rapidly to 72% at 24 h. After SO₂ was shut off, NO conversion increased slightly but could not be completely recovered. During the NO conversion process in the presence of SO₂, irreversible deactivation of the catalyst occurred. This result is attributed to the SO₂ transformation into ammonium sulfates with NH₃, blocking the active sites on the surface of the catalyst, and competition with NO for adsorption onto the active sites [21]. Furthermore, Figure 2b shows the results of the catalytic activity in the presence of H₂O (5 vol %) over Mn–Ce/Al₂O₃; when H₂O addition began, the NO conversions of Mn–Ce/Al₂O₃ decreased to ca. 13%. Over the next 23 h, the NO conversion was nearly unchanged and almost recovered to the initial activity after H₂O was removed, which resulted from the competitive adsorption between H₂O and NH₃/NO_x.

In addition, the stability of the Mn–Ce/Al₂O₃ catalyst was also tested at the same temperature and the results are presented in Figure 2c, indicating that there is no deactivation during the successive testing performed over the 168 h period at 100 °C in the absence of SO₂ and H₂O. Thus, the Mn–Ce/Al₂O₃ catalyst appears to be highly stable for NO elimination at low temperatures under the examined period of operation. Nevertheless, NO conversion by Mn–Ce/Al₂O₃ decreased quickly to 58% when SO₂ and H₂O were introduced into the gas flow simultaneously and the NO conversion was nearly stable over the next 124 h. The NO conversion then increased quickly to 70%, after the SO₂ and H₂O were removed. Meanwhile, the passivation effect was noticeably enhanced in the co-presence of SO₂ and H₂O because in the atmosphere with O₂ and H₂O, SO₂ reacts with NH₃ to form (NH₄)₂SO₄ and NH₄HSO₄, which are deposited on the catalyst surface, resulting in its deactivation [14]. According to the above results, it can be concluded that the Mn–Ce/Al₂O₃ catalyst exhibits some degree of SO₂ and H₂O resistance and that SO₂ has a more significant inhibiting effect on the NH₃-SCR catalytic activity than H₂O [22,23]. Combined with the NH₃-SCR effect of sulfation over this catalyst, we attempted to understand the interaction mechanism between SO₂ and the honeycomb cordierite-based Mn–Ce/Al₂O₃ catalyst.

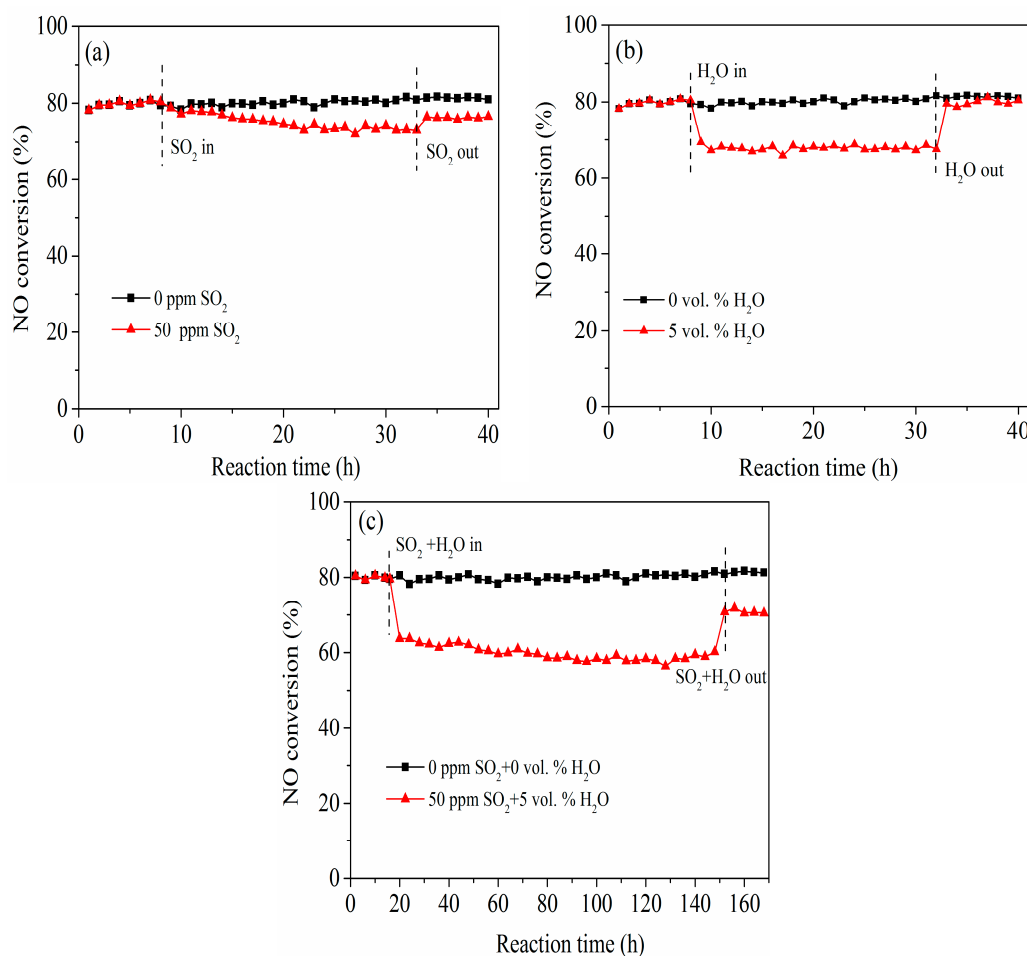


Figure 2. Effect of SO₂ and/or H₂O on NO removal activities of the honeycomb cordierite-based Mn–Ce/Al₂O₃ catalyst at 100 °C. (a) 50 ppm SO₂ resistance tests; (b) 5 vol % H₂O resistance tests; (c) 50 ppm SO₂ and 5 vol % H₂O resistance tests.

3.3. Physico-Chemical Characterization of Honeycomb Cordierite-Based Mn–Ce/Al₂O₃ Catalysts

3.3.1. BET, SEM-EDS Mapping

The surface area data of the fresh and sulfated samples are illustrated in Figure 3. Compared with that of the fresh Mn–Ce/Al₂O₃ catalyst, the BET surface area of the sulphated Mn–Ce/Al₂O₃ catalyst is decreased by 53.1%. Compared to those of S-Mn–Ce/Al₂O₃, the pore size and pore volume of F-Mn–Ce/Al₂O₃ are decreased by 27.6% and 37.1%, respectively. These results indicate that NO removal in the presence of SO₂ leads to a decrease in the BET surface area, pore size, and pore volume, which can be correlated with the formation of some species on the surface of the catalyst, which leads to the clogging of some of the catalyst pores.

SEM studies were conducted to investigate the change in morphology of the catalysts after the SCR reaction. The SEM images in Figure 4 demonstrate that the surface of the F-Mn–Ce/Al₂O₃ was smoother and more compact than those of R-Mn–Ce/Al₂O₃ and S-Mn–Ce/Al₂O₃. As shown in Figure 4, the surface of the F-Mn–Ce/Al₂O₃ catalyst is almost flat. However, after SO₂ (50 ppm) poisoning, a high degree of aggregation on the surface was observed (Figure 4a,c). Additionally, compared with F-Mn–Ce/Al₂O₃ (Figure 4a), there was no apparent change on the surface of the R-Mn–Ce/Al₂O₃ catalyst (Figure 4b), but a few depositions could be seen on S-Mn–Ce/Al₂O₃ (Figure 4c). This finding can be interpreted as a cause for the decrease in the surface area and pore volume (Figure 3). In addition, EDS displayed the Mn, Ce, Al, C, and O signals, further proving

that mixed metal oxide catalysts have been fabricated and supported on the honeycomb cordierite (Figure 4d). To further investigate the dispersion degree of the catalyst powder on the surface of the carrier, the SEM-EDS mapping of the F-Mn-Ce/Al₂O₃ is displayed in Figure 4e–h. The existence of Mn, Ce, Al, and O elements is clear, and high dispersion is shown (Figure 4e–g), indicating a well-mixed state of the catalyst. The above characteristics are also consistent with the analysis results of EDS.

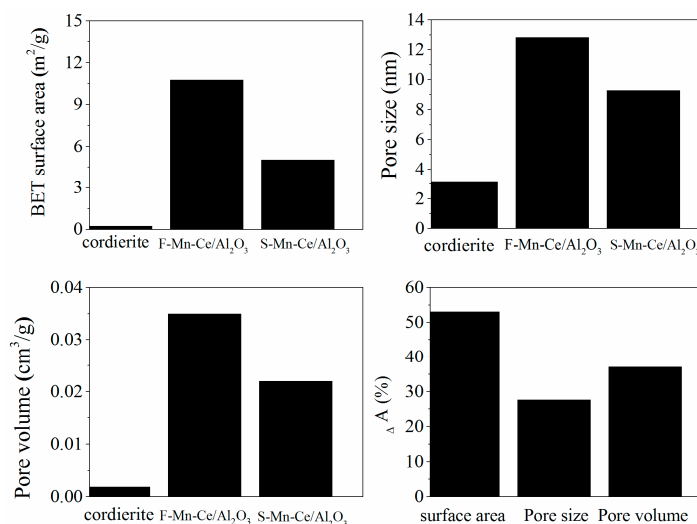


Figure 3. Brunauer–Emmet–Teller (BET) Surface Area, pore size, and pore volume of the fresh (F) and sulfated (S) honeycomb cordierite-based Mn–Ce/Al₂O₃ catalysts ($\Delta A = (A_F - A_S/A_F) \times 100\%$).

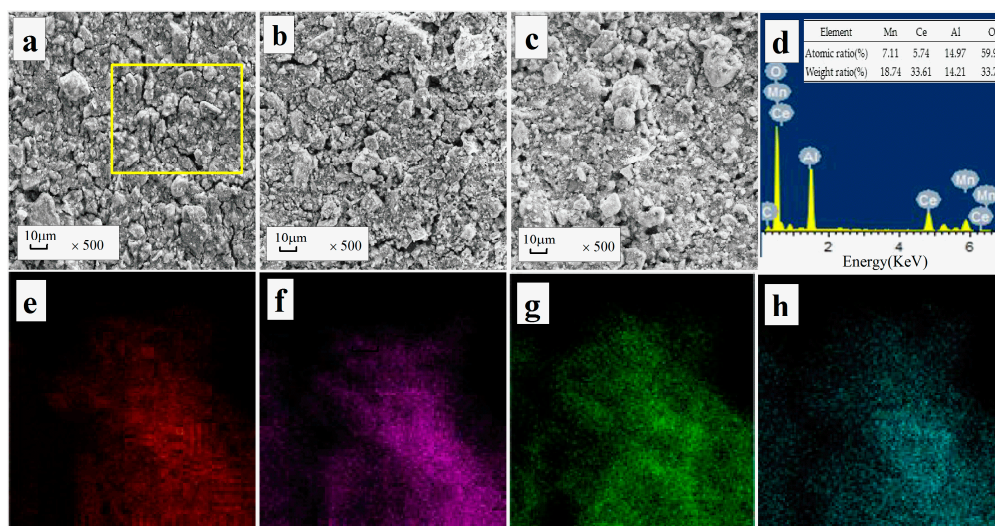


Figure 4. (a–c) Scanning electron microscopy (SEM) images of fresh and SO₂ poisoned catalysts and (d–h) SEM-Energy dispersive spectroscopy (EDS) element mapping of fresh catalyst. (a) F-Mn–Ce/Al₂O₃; (b) R-Mn–Ce/Al₂O₃; (c) S-Mn–Ce/Al₂O₃; and (d) EDS spectra of the Mn–Ce/Al₂O₃ particles in yellow panel (a); (e) Mn; (f) Ce; (g) Al, (h) O.

Figure 5 shows the N₂ adsorption–desorption isotherms and pore size distribution of the fresh and poisoned catalysts, in which the isotherms are classical type IV [24]. The H2-type hysteresis loop was observed, which is typical for a wormhole-like mesostructure [18]. In addition, the beginning and end of the adsorption volume shifted in the direction of a large p/p_0 , which shows that there was some smaller pore clogging of the catalyst after poisoning by SO₂.

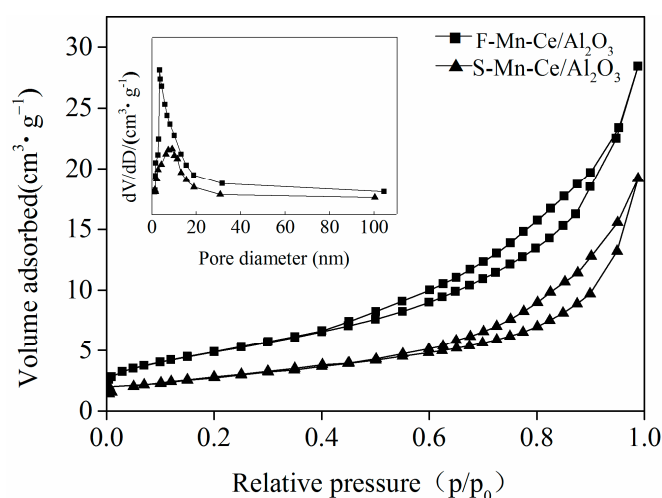


Figure 5. N_2 adsorption–desorption isotherms and Barrett-Joyner-Halenda (BJH) pore size distribution of Mn–Ce/ Al_2O_3 before (F) and after (S) poisoning by SO_2 .

To further understand the microstructure of the poisoned Mn–Ce/ Al_2O_3 , XRD analysis was performed. The XRD patterns of the honeycomb cordierite-based Mn–Ce/ Al_2O_3 catalysts before and after the reaction are depicted in Figure 6. Several diffraction peaks observed at 28.95° , 33.29° , 47.49° , 57.16° , and 76.71° could be assigned to a cubic CeO_2 crystallite (PDF#34-0394). The peaks attributed to CeO_2 could also be seen before and after the SCR reaction [25]. However, no manganese oxide phases could be detected, indicating that the manganese oxides formed as primary crystals of less than approximately 4 nm, which was consistent with the report by Machida et al. [26]. After the reaction, there were no new peaks that emerged on the S-Mn–Ce/ Al_2O_3 XRD curve, which indicated that no crystal sulfate phase was formed on Mn–Ce/ Al_2O_3 after the reaction or that the surface sulphate amount was below the detection limit [27].

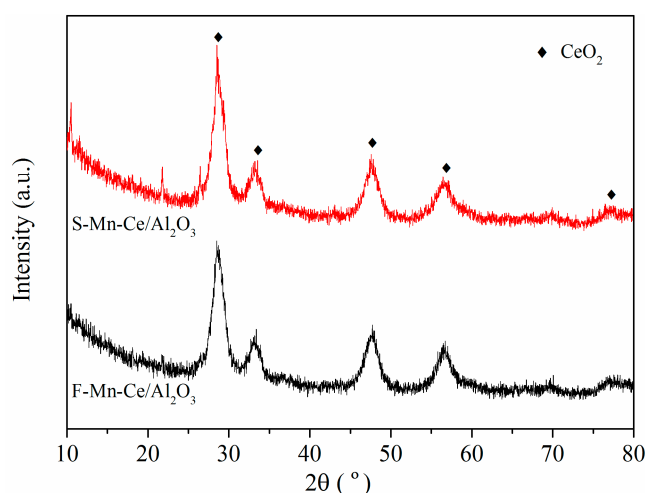


Figure 6. X-ray diffraction (XRD) patterns of Mn–Ce/ Al_2O_3 before (F) and after (S) poisoning by SO_2 .

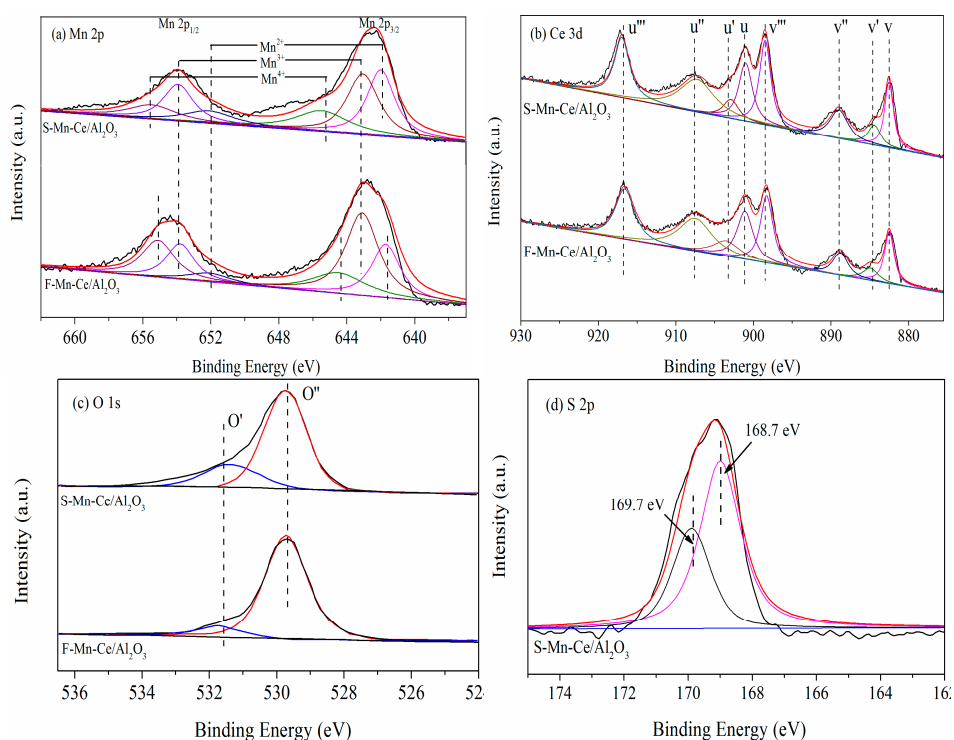
3.3.2. XPS

XPS experiments were performed to investigate the surface component and chemical state change of elements over the fresh and sulfated catalysts. The surface atomic concentrations of Mn, Ce, O, and S are summarized in Table 1, and the photoelectron spectra of the Mn 2p, Ce 3d, O 1s, and S 2p levels are displayed in Figure 7.

Table 1. Surface atomic distributions of the catalysts by X-ray photoelectron spectroscopy (XPS).

Samples	Atomic Concentration (at %)				Surface Atomic Ratio (%)		
	Mn	Ce	O	S	Ce ³⁺ /(Ce ³⁺ + Ce ⁴⁺)	Mn ⁴⁺ /(Mn ²⁺ + Mn ³⁺ + Mn ⁴⁺)	O'/O' + O''
F-Mn-Ce/Al ₂ O ₃	7.31	2.49	55.21	0	11.6	35.6	15.8
S-Mn-Ce/Al ₂ O ₃	4.05	1.99	66.75	3.01	12.7	26.74	30.5

The Mn 2p XPS spectra of the fresh and sulphated Mn-Ce/Al₂O₃ samples are shown in Figure 7a. Two peaks, due to Mn 2p_{1/2} and Mn 2p_{3/2}, were observed from 637.0 eV to 662.5 eV, which are characteristic of a mixed-manganese system (Mn²⁺, Mn³⁺, and Mn⁴⁺) [28]. The Mn 2p XPS spectra of the F-Mn-Ce/Al₂O₃ could be classified into six subpeaks: Mn²⁺ (641.6 and 652.1 eV), Mn³⁺ (643.1 and 653.9 eV), and Mn⁴⁺ (644.2 and 655.1 eV) [29], indicating that Mn²⁺, Mn³⁺, and Mn⁴⁺ co-exist on the surface of the catalysts. Compared with F-Mn-Ce/Al₂O₃, the Mn 2p peak for the poisoned S-Mn-Ce/Al₂O₃ slightly shifted to a higher binding energy (0.2–0.5 eV higher), which may be attributed to the formation of species other than manganese oxides for Mn-Ce/Al₂O₃, which could occur when catalysts are sulfated, shifting them to a higher binding energy [30]. Here, the binding energies were shifted higher during the SCR reaction in the presence of SO₂, which means that the Mn species on the surface of the Mn-Ce/Al₂O₃ catalyst were less active, thus resulting in performance degradation. In addition, Kapteijn et al. [31] demonstrated that Mn⁴⁺ has a better redox ability than Mn²⁺ and Mn³⁺ over the spectrum of manganese-based catalysts. For the two samples, the ratio Mn⁴⁺/(Mn²⁺+Mn³⁺+Mn⁴⁺) can be calculated from the characteristic peaks intensities of Mn²⁺, Mn³⁺, and Mn⁴⁺. The ratio of Mn⁴⁺/(Mn²⁺+Mn³⁺+Mn⁴⁺) decreased by 8.86% for F-Mn-Ce/Al₂O₃ and S-Mn-Ce/Al₂O₃. Therefore, the decreased concentration of Mn⁴⁺ can also reflect the reason for the activity decrease.

**Figure 7.** X-ray photoelectron spectroscopy (XPS) spectra of the catalysts before and after 24 h of an SO₂-containing reaction at 100 °C. (a) Mn 2p; (b) Ce 3d; (c) O 1s; and (d) S 2p.

The complicated Ce 3d XPS spectra of the fresh and sulphated Mn-Ce/Al₂O₃ catalyst are presented in Figure 7b. The bands labelled u and v are representative of the 3d_{3/2} spin-orbit states

and $3d_{5/2}$ states, respectively. The peaks assigned u' and v' are representative of the $3d^{10}4f^1$ electronic state of Ce^{3+} ions, while u , u'' , u''' and v , v'' , v''' are attributed to the $3d^{10}4f^0$ state of the Ce^{4+} species [32,33]. The intensities of the Ce^{3+} peaks slightly increased after the SCR reaction in the presence of SO_2 . The concentration of Ce^{3+} was used to evaluate the number of formed oxygen vacancies. The oxygen vacancies were driven by the transition from Ce^{4+} to Ce^{3+} , which accelerated the transport of active oxygen species [18] and facilitated the reaction. The ratio of $Ce^{3+}/(Ce^{3+}+Ce^{4+})$ over the used sample (12.7%) was slightly greater than that of the fresh sample (11.6%) (Table 1), due to the following reaction [34,35]: $2CeO_2 + 3SO_2 + O_2 \rightarrow Ce_2(SO_4)_3$. Since the generated $Ce_2(SO_4)_3$ on the surface of the Mn–Ce/ Al_2O_3 catalyst does not decompose at 100 °C, the $Ce_2(SO_4)_3$ would lead to a reduction of the NO conversion (Figure 2). Figure 7c shows the O1s XPS spectra of the fresh and used Mn–Ce/ Al_2O_3 samples. The spectra could be fitted into two sub-bands, the first sub-band at 531.3–532.2 eV corresponding to the surface chemisorbed oxygen (O'), similar to O_2^{2-} pertaining to the defect-oxide or hydroxyl-like groups [36], and the second sub-band at 528.5–530.5 eV corresponding to the lattice oxygen O^{2-} (O'') [37]. After sulfation, there was a significant increase in the ratio of $O'/(O' + O'')$ in S-Mn–Ce/ Al_2O_3 , which was due to the oxygen of the sulfate or the hydroxyl on the surface. Moreover, the accumulation of O' might result in a suppressed effect in the adsorption and desorption of NO [38]; the adsorption, transformation, and desorption of NO were the controlling steps of the SCR reaction. Consequently, the catalyst activity significantly decreased after SO_2 poisoning. The S 2p XPS of the sulphated Mn–Ce/ Al_2O_3 catalyst (Figure 7d) had two sub-peaks at 168.7 eV and 169.7 eV, assigned to the SO_3^{2-} and SO_4^{2-} species, respectively [39,40]. This result confirmed that sulfate species were formed over the sulphated Mn–Ce/ Al_2O_3 .

3.3.3. TG-DTA

To distinguish the different sulfate species formed during the sulfation process, the fresh and used catalysts were examined using TG-DTA.

Figure 8a shows the TG and Differential Scanning Calorimetry (DSC) curves of F-Mn–Ce/ Al_2O_3 , in which the TG curve presented one primary weight loss at approximately 80 °C, with the DSC curve revealing a corresponding valley. The weight loss was attributed to the desorption of adsorbed water on the catalyst [41]. In the TG-DTA curves of S-Mn–Ce/ Al_2O_3 (Figure 8b), there are three main weight losses at approximately 80 °C, 370 °C, and 790 °C. The weight loss at 370 °C was attributed to the decomposition of NH_4HSO_4 into $(NH_4)_2S_2O_7$ and H_2O , and the $(NH_4)_2S_2O_7$ decomposition generated NH_3 , SO_2 , H_2O , and N_2 , as reported in the literature [42,43]. According to the report, the decomposition temperature of $Ce_2(SO_4)_3$ or $Ce(SO_4)_2$ was greater than 700 °C [34]. Therefore, sulfated CeO_2 decomposition or desorption can explain the weight loss peak at 790 °C. Upon completion of the TG-DTA analysis, it can be concluded that ammonium hydrogen sulfate and sulfated CeO_2 were formed during the reaction process in the presence of SO_2 .

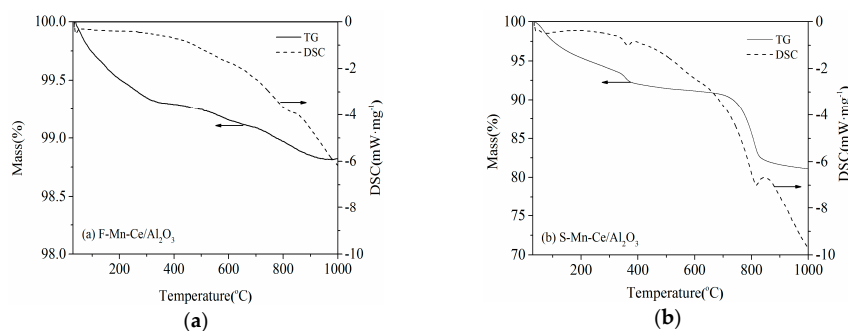


Figure 8. Thermogravimetry and Differential Thermal Analysis (TG-DTA) curves of fresh and used catalysts: (a) F-Mn–Ce/ Al_2O_3 ; (b) S-Mn–Ce/ Al_2O_3 .

3.3.4. FT-IR Analysis

Further confirmation of the TG-DTA data was obtained by FT-IR analysis to investigate the sulfate and ammonium groups on the catalyst surface. Figure 9 shows the FT-IR spectra of fresh and used catalysts.

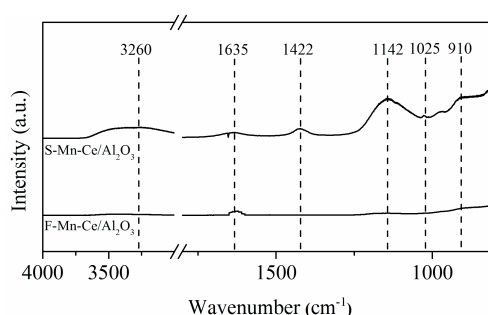


Figure 9. Fourier transform infrared (FT-IR) spectra of fresh (F) and used (S) Mn–Ce/Al₂O₃ catalyst.

The fresh and used catalyst both exhibited bands at 910 and 1635 cm⁻¹ and featured different metal oxides. In comparison with the fresh Mn–Ce/Al₂O₃, the used Mn–Ce/Al₂O₃ revealed some new bands at 1025, 1142, 1422, and 3260 cm⁻¹. According to literature [44–46], the bands at 1025 and 1142 cm⁻¹ were assigned to the antisymmetric stretching vibration of the SO₄²⁻ group [47]. The peak at 1422 cm⁻¹ indicated the presence of NH₄⁺ species, adsorbed on the Brønsted acid sites [46,48]. Additionally, the broad peak at 3260 cm⁻¹ was attributed to the N–H stretching vibration of the NH₄⁺ group [49]. Combining the TG-DTA result with the FT-IR result, the conclusion further confirms that the formation of sulfate species on the surface of the catalyst during the SCR reaction in the presence of SO₂ can lead to pore plugging, a decrease in the surface area, and occupation of the active sites, which explain the decline in the SCR activity of the catalyst [18].

4. Conclusions

In the present work, the poisoning effect of SO₂ on the honeycomb cordierite-based Mn–Ce/Al₂O₃ catalyst performance and the physicochemical properties were studied. The honeycomb cordierite-based Mn–Ce/Al₂O₃ catalyst showed satisfactory catalytic activity at 100 °C in the presence of SO₂. However, the catalytic activity decreased to 72% after a 24 h reaction. The physicochemical characterization results indicated that the ammonium hydrogen sulfate and sulfated CeO₂ were formed and were deposited on the surface of the honeycomb cordierite-based Mn–Ce/Al₂O₃ catalysts during the NH₃-SCR process in the presence of SO₂. This process could result in blocking the pores of the catalyst and decreasing the surface area, thus decreasing the SCR activity. In addition, larger losses of Mn and Ce occur on the surface of sulphated Mn–Ce/Al₂O₃ than on that of fresh Mn–Ce/Al₂O₃, directly leading to the decreased NO_x removal ability.

Acknowledgments: This work was financially supported by the National High Technology Research and Development Program of China (2015AA03A401).

Author Contributions: C.Z. and P.C. conceived and designed the experiments; C.W. performed the experiments; Y.Z. and X.Y. analyzed the data; C.W. wrote the paper.

Conflicts of Interest: The authors declare no conflicts of interest.

References

1. Liu, Z.; Yang, Y.; Zhang, S.; Zhu, T.; Zhu, J.; Wang, J. Selective catalytic reduction of NO_x with NH₃ over Mn–Ce mixed oxide catalyst at low temperatures. *Catal. Today* **2013**, *216*, 76–81. [[CrossRef](#)]
2. Zhang, J.; Qu, H. Low-temperature selective catalytic reduction of NO_x with NH₃ over Fe–Cu mixed oxide/ZSM-5 catalysts containing Fe₂CuO₄ phase. *Res. Chem. Intermed.* **2015**, *41*, 4961–4975. [[CrossRef](#)]

3. Boningari, T.; Smirniotis, P.G. Impact of nitrogen oxides on the environment and human health: Mn-based materials for the NO_x abatement. *Curr. Opin. Chem. Eng.* **2016**, *13*, 133–141. [[CrossRef](#)]
4. Shen, B.; Liu, T.; Zhao, N.; Yang, X.; Deng, L. Iron-doped Mn-Ce/TiO₂ catalyst for low temperature selective catalytic reduction of NO with NH₃. *J. Environ. Sci.* **2010**, *22*, 1447–1454. [[CrossRef](#)]
5. Zhang, Q.; Qiu, C.; Xu, H.; Lin, T.; Lin, Z.; Gong, M.; Chen, Y. Low-temperature selective catalytic reduction of NO with NH₃ over monolith catalyst of MnO_x/CeO₂-ZrO₂-Al₂O₃. *Catal. Today* **2011**, *175*, 171–176. [[CrossRef](#)]
6. Liang, Q.; Li, J.; He, H.; Liang, W.; Zhang, T.; Fan, X. Effects of SO₂ on the low temperature selective catalytic reduction of NO by NH₃ over CeO₂-V₂O₅-WO₃/TiO₂ catalysts. *Front. Environ. Sci. Eng.* **2017**, *11*, 4. [[CrossRef](#)]
7. Li, J.; Chang, H.; Ma, L.; Hao, J.; Yang, R.T. Low-temperature selective catalytic reduction of NO_x with NH₃ over metal oxide and zeolite catalysts—A review. *Catal. Today* **2011**, *175*, 147–156. [[CrossRef](#)]
8. Sheng, Z.; Hu, Y.; Xue, J.; Wang, X.; Liao, W. SO₂ poisoning and regeneration of Mn-Ce/TiO₂ catalyst for low temperature NO_x reduction with NH₃. *J. Rare Earths* **2012**, *30*, 676–682. [[CrossRef](#)]
9. Huang, J.; Tong, Z.; Huang, Y.; Zhang, J. Selective catalytic reduction of NO with NH₃ at low temperatures over iron and manganese oxides supported on mesoporous silica. *Appl. Catal. B Environ.* **2008**, *78*, 309–314. [[CrossRef](#)]
10. Liu, C.; Shi, J.W.; Gao, C.; Niu, C. Manganese oxide-based catalysts for low-temperature selective catalytic reduction of NO_x with NH₃: A review. *Appl. Catal. A Gen.* **2016**, *522*, 54–69. [[CrossRef](#)]
11. Wu, Z.; Jin, R.; Liu, Y.; Wang, H. Ceria modified MnO_x/TiO₂ as a superior catalyst for NO reduction with NH₃ at low-temperature. *Catal. Commun.* **2008**, *9*, 2217–2220. [[CrossRef](#)]
12. Zhang, L.; Cui, S.; Guo, H.; Ma, X.; Luo, X. The influence of K⁺ cation on the MnO_x-CeO₂/TiO₂ catalysts for selective catalytic reduction of NO_x with NH₃ at low temperature. *J. Mol. Catal. A Chem.* **2014**, *390*, 14–21. [[CrossRef](#)]
13. Jin, Q.; Shen, Y.; Zhu, S. Effect of fluorine additive on CeO₂ZrO₂/TiO₂ for selective catalytic reduction of NO by NH₃. *J. Colloid Interface Sci.* **2016**, *487*, 401. [[CrossRef](#)] [[PubMed](#)]
14. Cao, F.; Su, S.; Xiang, J.; Wang, P.Y.; Hu, S.; Sun, L.S.; Zhang, A.C. The activity and mechanism study of Fe-Mn-Ce/gamma-Al₂O₃ catalyst for low temperature selective catalytic reduction of NO with NH₃. *Fuel* **2015**, *139*, 232–239. [[CrossRef](#)]
15. Tang, C.; Zhang, H.; Dong, L. Ceria-based catalysts for low-temperature selective catalytic reduction of NO with NH₃. *Catal. Sci. Technol.* **2016**, *6*, 1248–1264. [[CrossRef](#)]
16. Smirniotis, P.G.; Peña, D.A.; Uphade, B.S. Low-Temperature Selective Catalytic Reduction (SCR) of NO with NH₃ by Using Mn, Cr, and Cu Oxides Supported on Hombikat TiO₂. *Angew. Chem. Int. Ed.* **2010**, *40*, 2479–2482. [[CrossRef](#)]
17. Thirupathi, B.; Smirniotis, P.G. Nickel-doped Mn/TiO₂ as an efficient catalyst for the low-temperature SCR of NO with NH₃: Catalytic evaluation and characterizations. *J. Catal.* **2012**, *288*, 74–83. [[CrossRef](#)]
18. Xiong, Y.; Tang, C.; Yao, X.; Zhang, L.; Li, L.; Wang, X.; Deng, Y.; Gao, F.; Lin, D. Effect of metal ions doping (M = Ti⁴⁺, Sn⁴⁺) on the catalytic performance of MnO_x/CeO₂ catalyst for low temperature selective catalytic reduction of NO with NH₃. *Appl. Catal. A Gen.* **2015**, *495*, 206–216. [[CrossRef](#)]
19. Kijlstra, W.S.; Brands, D.S.; Poels, E.K.; Bliiek, A. Kinetics of the selective catalytic reduction of NO with NH₃ over MnO_x/Al₂O₃ catalysts at low temperature. *Catal. Today* **1999**, *50*, 133–140. [[CrossRef](#)]
20. Wu, Z.; Jin, R.; Wang, H.; Liu, Y. Effect of ceria doping on SO₂ resistance of Mn/TiO₂ for selective catalytic reduction of NO with NH₃ at low temperature. *Catal. Commun.* **2009**, *10*, 935–939. [[CrossRef](#)]
21. Jin, R.; Liu, Y.; Wu, Z.; Wang, H.; Gu, T. Relationship between SO₂ poisoning effects and reaction temperature for selective catalytic reduction of NO over Mn-Ce/TiO₂ catalyst. *Catal. Today* **2010**, *153*, 84–89. [[CrossRef](#)]
22. Li, L.; Zhang, L.; Ma, K.; Zou, W.; Cao, Y.; Xiong, Y.; Tang, C.; Lin, D. Ultra-low loading of copper modified TiO₂/CeO₂ catalysts for low-temperature selective catalytic reduction of NO by NH₃. *Appl. Catal. B Environ.* **2017**, *207*, 366–375. [[CrossRef](#)]
23. Mach, P.; Kocian, M. Combination of Experimental and Theoretical Investigations of MnO_x/Ce_{0.9}Zr_{0.1}O₂ Nanorods for Selective Catalytic Reduction of NO with Ammonia. *J. Phys. Chem. C* **2013**, *117*, 9999–10006. [[CrossRef](#)]
24. Sing, K.S.W. Reporting physisorption data for gas/solid systems with special reference to the determination of surface area and porosity (recommendations 1984). *Pure Appl. Chem.* **1985**, *57*, 603–619. [[CrossRef](#)]

25. Wang, Y.; Ge, C.Z.; Zhan, L.; Li, C.; Qiao, W.; Ling, L. MnO_x-CeO₂/activated carbon honeycomb catalyst for selective catalytic reduction of NO with NH₃ at low temperatures. *Ind. Eng. Chem. Res.* **2012**, *51*, 11667–11673. [[CrossRef](#)]
26. Machida, M.; Daisuke Kurogi, A.; Kijima, T. MnO_x-CeO₂ binary oxides for catalytic NO_x-sorption at low temperatures. Selective reduction of sorbed NO_x. *Chem. Mater.* **2000**, *12*, 3158–3164. [[CrossRef](#)]
27. Zhou, A.; Yu, D.; Yang, L.; Sheng, Z. Combined effects Na and SO₂ in flue gas on Mn-Ce/TiO₂ catalyst for low temperature selective catalytic reduction of NO by NH₃ simulated by Na₂SO₄ doping. *Appl. Surf. Sci.* **2016**, *378*, 167–173. [[CrossRef](#)]
28. Zhang, X.; Ji, L.; Zhang, S.; Yang, W. Synthesis of a novel polyaniline-intercalated layered manganese oxide nanocomposite as electrode material for electrochemical capacitor. *J. Power Sources* **2007**, *173*, 1017–1023. [[CrossRef](#)]
29. Reddy, A.S.; Gopinath, C.S.; Chilukuri, S. Selective ortho -methylation of phenol with methanol over copper manganese mixed-oxide spinel catalysts. *J. Catal.* **2006**, *243*, 278–291. [[CrossRef](#)]
30. Venezia, A.M.; Carlo, G.D.; Pantaleo, G.; Liotta, L.F.; Melaet, G.; Kruse, N. Oxidation of CH₄ over Pd supported on TiO₂-doped SiO₂: Effect of Ti(IV) loading and influence of SO₂. *Appl. Catal. B Environ.* **2009**, *88*, 430–437. [[CrossRef](#)]
31. Kapteijn, F.; Singoredjo, L.; Andreini, A.; Moulijn, J.A. Cheminform abstract: Activity and selectivity of pure manganese oxides in the selective catalytic reduction of nitric oxide with ammonia. *Cheminform* **1994**, *3*, 173–189. [[CrossRef](#)]
32. Li, P.; Xin, Y.; Li, Q.; Wang, Z.; Zhang, Z.; Zheng, L. Ce-Ti amorphous oxides for selective catalytic reduction of NO with NH₃: Confirmation of Ce-O-Ti active sites. *Environ. Sci. Technol.* **2012**, *46*, 9600–9605. [[CrossRef](#)] [[PubMed](#)]
33. Ilieva, L.; Tabakova, T.; Pantaleo, G.; Ivanov, I.; Zanella, R.; Paneva, D.; Velinov, N.; Sobczak, J.W.; Lisowski, W.; Avdeev, G. Nano-gold catalysts on Fe-modified ceria for pure hydrogen production via wgs and prox: Effect of preparation method and Fe-doping on the structural and catalytic properties. *Appl. Catal. A Gen.* **2013**, *467*, 76–90. [[CrossRef](#)]
34. Xu, W.; He, H.; Yu, Y. Deactivation of a Ce/TiO₂ catalyst by SO₂ in the selective catalytic reduction of NO by NH₃. *J. Phys. Chem. C* **2009**, *113*, 4426–4432. [[CrossRef](#)]
35. Liu, Z.; Zhu, J.; Zhang, S.; Ma, L.; Woo, S.I. Selective catalytic reduction of NO_x by NH₃ over MoO₃-promoted CeO₂/TiO₂ catalyst. *Catal. Commun.* **2014**, *46*, 90–93. [[CrossRef](#)]
36. Chang, H.; Chen, X.; Li, J.; Ma, L.; Wang, C.; Liu, C.; Schwank, J.W.; Hao, J. Improvement of activity and SO₂ tolerance of Sn-modified MnO_x-CeO₂ catalysts for NH₃-SCR at low temperatures. *Environ. Sci. Technol.* **2013**, *47*, 5294–5301. [[CrossRef](#)] [[PubMed](#)]
37. Yao, X.; Zhang, L.; Li, L.; Liu, L.; Cao, Y.; Dong, X.; Gao, F.; Yu, D.; Tang, C.; Chen, Z. Investigation of the structure, acidity, and catalytic performance of CuO/Ti_{0.95}Ce_{0.05}O₂ catalyst for the selective catalytic reduction of NO by NH₃ at low temperature. *Appl. Catal. B Environ.* **2014**, *150–151*, 315–329. [[CrossRef](#)]
38. Chen, B.; Yunsheng, M.A.; Ding, L.; Lingshun, X.U.; Zongfang, W.U.; Yuan, Q.; Huang, W. XPS and TPD study of NO interaction with Cu(111): Role of different oxygen species. *Chin. J. Catal.* **2013**, *34*, 964–972. [[CrossRef](#)]
39. Pan, S.; Luo, H.; Li, L.; Wei, Z.; Huang, B. H₂O and SO₂ deactivation mechanism of MnO_x/MWCNTs for low-temperature SCR of NO_x with NH₃. *J. Mol. Catal. A Chem.* **2013**, *377*, 154–161. [[CrossRef](#)]
40. Hino, M.; Kurashige, M.; Matsushige, H.; Arata, K. The surface structure of sulfated zirconia: Studies of XPS and thermal analysis. *Thermochim. Acta* **2006**, *441*, 35–41. [[CrossRef](#)]
41. Li, X.; Zhang, S.; Jia, Y.; Liu, X.; Zhong, Q. Selective catalytic oxidation of NO with over Ce-doped MnO/TiO catalysts. *J. Nat. Gas Chem.* **2012**, *21*, 17–24. [[CrossRef](#)]
42. Alemany, L.J.; Berti, F.; Busca, G.; Ramis, G.; Robba, D.; Toledo, G.P.; Trombetta, M. Characterization and composition of commercial V₂O₅ and W₂O₅/TiO₂ SCR catalysts. *Appl. Catal. B Environ.* **1996**, *10*, 299–311. [[CrossRef](#)]
43. Bai, S.; Zhao, J.; Wang, L.; Zhu, Z. SO₂-promoted reduction of NO with NH₃ over vanadium molecularly anchored on the surface of carbon nanotubes. *Catal. Today* **2010**, *158*, 393–400. [[CrossRef](#)]
44. Pietrogioacomi, D.; Magliano, A.; Ciambelli, P.; Sannino, D.; Campa, M.C.; Indovina, V. The effect of sulphation on the catalytic activity of CoO_x/ZrO₂ for NO reduction with NH₃ in the presence of O₂. *Appl. Catal. B Environ.* **2009**, *89*, 33–40. [[CrossRef](#)]

45. Seo, P.W.; Park, K.H.; Hong, S.C. SO₂ durability enhancement of ball milled V/TiO₂ catalyst. *J. Ind. Eng. Chem.* **2010**, *16*, 283–287. [[CrossRef](#)]
46. Yu, J.; Guo, F.; Wang, Y.; Zhu, J.; Liu, Y.; Su, F.; Gao, S.; Xu, G. Sulfur poisoning resistant mesoporous Mn-base catalyst for low-temperature SCR of NO with NH₃. *Appl. Catal. B Environ.* **2010**, *95*, 160–168. [[CrossRef](#)]
47. Nakamoto, K. *Infrared and Raman Spectra of Inorganic and Coordination Compounds*; Wiley: Hoboken, NJ, USA, 1986; p. 1122. [[CrossRef](#)]
48. Topsøe, N.Y. Mechanism of the selective catalytic reduction of nitric oxide by ammonia elucidated by in situ online fourier transform infrared spectroscopy. *Science* **1994**, *265*, 1217. [[CrossRef](#)] [[PubMed](#)]
49. Xie, G.; Liu, Z.; Zhu, Z.; Liu, Q.; Ge, J.; Huang, Z. Simultaneous removal of SO₂ and NO_x from flue gas using a CuO/Al₂O₃ catalyst sorbent: I. Deactivation of SCR activity by SO₂ at low temperatures. *J. Catal.* **2004**, *224*, 36–41. [[CrossRef](#)]



© 2018 by the authors. Licensee MDPI, Basel, Switzerland. This article is an open access article distributed under the terms and conditions of the Creative Commons Attribution (CC BY) license (<http://creativecommons.org/licenses/by/4.0/>).